Steel and Composite Structures, *Vol. 33, No. 2* (*2019*) *245-259*
DOI: https://doi.org/10.12989/scs.2019.33.2.245

Combined effects of end-shortening strain, lateral pressure load and initial imperfection on ultimate strength of laminates: nonlinear plate theory

S.A.M. Ghannadpour* and A. Kurkaani Barvaj

New Technologies and Engineering Department, *Shahid Beheshti University*, *G.C*, *Tehran*, *Iran*

(*Received May 3, 2019, Revised September 24, 2019, Accepted October 2, 2019*)

Abstract. The present study aims to investigate the ultimate strength and geometric nonlinear behavior of composite plates containing initial imperfection subjected to combined end-shortening strain and lateral pressure loading by using a semi-analytical method. In this study, the first order shear deformation plate theory is considered with the assumption of large deflections. Regarding in-plane boundary conditions, two adjacent edges of the laminates are completely held while the two others can move straightly. The formulations are based on the concept of the principle of minimum potential energy and Newton-Raphson technique is employed to solve the nonlinear set of algebraic equations. In addition, Hashin failure criteria are selected to predict the failures. Further, two distinct models are assumed to reduce the mechanical properties of the failure location, complete ply degradation model, and ply region degradation model. Degrading the material properties is assumed to be instantaneous. Finally, laminates having a wide range of thicknesses and initial geometric imperfections with different intensities of pressure load are analyzed and discuss how the ultimate strength of the plates changes.

Keywords: ultimate strength; geometric nonlinearity; lateral pressure; initial imperfection; Ritz method; Hashin criteria

1. Introduction

The composite layered panels with fibers are widely used in shipbuilding, aerospace industry, and marine engineering. The panels used in the form of thin plates are exposed to various loadings and boundary conditions. These panels are often employed in situation where they are subjected to in-plane compressive loading. Thus, the prediction of the buckling and post-buckling behavior of such structures is highly important. Without considering failures and damage, the post-buckling and nonlinear analyses of these structures are very conservative and usually give inaccurate estimates of loads and deflections. Hence, analyzing the damage and finding ultimate strength of such structures have attracted a lot of attention.

A large number of studies have been conducted in the arena of buckling, post-buckling, and geometric nonlinear analyses of composite and functionally graded structures. Regarding buckling analysis, the relevant solutions for isotropic plates can be observed in the monograph of (Timoshenko and Gere 2009). Argyris and Tenek (1997) extensively reviewed the studies of buckling and post-buckling of structures by different methods. Becheri *et al*. (2016) investigated the buckling of symmetrically composite plates by nth-order shear deformation theory with curvature effect by an exact and analytical solution. Sun *et al*. (2016) studied the buckling and post-buckling thermomechanical deformations of a functionally graded material (FGM) Timoshenko beam resting on a two-parameter non-linear elastic foundation and subjected to only a temperature rise have been numerically investigated with the shooting method. Taheri-Behrooz *et al*. (2017) compared experimental and numerical results from buckling behavior of composite cylinders containing cutout. They have considered the effects of initial geometric imperfection in their analysis. In another research, Ghaheri *et al*. (2014) investigated buckling and vibration of thin symmetrically laminated composite elliptical plates on Winkler-type elastic foundation subjected to uniform in-plane edge loads based on the classical laminated plate theory. Nejati *et al*. (2017) examined thermal buckling of nanocomposite stiffened cylindrical shells reinforced by functionally graded wavy carbon nanotubes stiffened by stringers and rings subjected to a thermal loading with temperature-dependent properties. Further, Ghannadpour *et al*. (2017) investigated the geometrically nonlinear analyses of laminated composite plates with and without geometric imperfections based on pseudo spectral approach and using Legendre Basis Functions (LBF). Ghannadpour and Barekati also evaluated initial imperfection effects on the post-buckling response of laminated plates under end-shortening strain using Chebyshev techniques (Ghannadpour and Barekati 2016). In another study, Ghannadpour *et al*. (2014) examined buckling and post-buckling of relatively thick and symmetrically cross-ply laminated plates by using the exact finite strip method. In addition, Ovesy *et al*. (2015) evaluated the post-buckling behaviors of functionally graded rectangular plates in

*Corresponding author, Ph.D.,
E-mail: a_ghannadpour@sbu.ac.ir

ISSN: 1229-9367 (Print), 1598-6233 (Online)

thermal environments by using semi-analytical finite strip method. In another study, Ovesy *et al*. (2005) reported the post-buckling response of rectangular composite laminated plates with initial imperfections, when exposed to progressive end-shortening based on two different versions of finite strip method. Jiang *et al*. (2016) investigated the nonlinear vibrations analysis of composite laminated trapezoidal plates using the finite element method (FEM). Ghannadpour and Ovesy (2009a) investigated the buckling analysis of symmetrically laminated composite plates and prismatic plate structures by using exact finite strip method. Further, they emphasized the buckling and initial post-buckling analyses of channel section (Ovesy and Ghannadpour 2011) and box section struts using the exact finite strip method (Ghannadpour and Ovesy 2009b). Magnucki *et al*. (2006) studied the bending and buckling of a rectangular porous plate based on nonlinear displacement functions taking into account shearing deformations. Li *et al*. (2007) examined vibration of thermally post-buckled orthotropic circular plates. They have studied axisymmetric vibrations of a statically buckled polar orthotropic circular plate due to uniform temperature rise. The applicability of a new extended layerwise approach has been investigated by Topal (2013) for thermal buckling load optimization of laminates. A large number of studies have also been conducted with respect to the buckling and post-buckling analysis of composite structures using Finite Element Method (FEM). For example, Kar and Panda (2016) studied post-buckling behavior of shear deformable functionally graded curved shell panels of different shell geometry (spherical, elliptical, cylindrical and hyperbolic) under edge compression. Panda and Singh (2013) investigated nonlinear free vibration of thermally post-buckled laminated composite spherical shell panel embedded with shape memory alloy (SMA) fiber.

However, almost all of the studies related to the post-buckling analysis of the plates were conducted without considering the effects of damage and the results were conservative. Thus, the present study aimed to evaluate both geometric nonlinearity and progressive damage analyses of imperfect composite plates subjected to end-shortening and lateral pressure loading. Finite element method has often been used in the ultimate strength analyses of composite plates. Aghaei *et al*. (2015) studied the different failure criteria to predict damage in glass/polyester composite beams under low velocity impact implemented in ABAQUS software. Jiang *et al*. (2018) presented a research on evaluations of failure initiation criteria for predicting damages of composite structures under crushing loading. They studied the crushing behaviors of thin-walled composite structures subjected to quasi-static axial loading using four different failure initiation criteria.

However, it should be noted that conducting nonlinear and progressive damage analyzes by finite element method is a very time-consuming procedure. Tornabene *et al*. (2017) studied linear static behavior of damaged laminated composite plates and shells. In their study, a mathematical procedure was proposed to model a damaged mechanical configuration for composite laminated and sandwich structures. Brubak and Hellesland (2007a) and Brubak *et al*. (Brubak and Hellesland 2007b, 2008, Brubak *et al*. 2007) developed a group of simplified methods in order to analyze the buckling and ultimate strength of metal plates with and without stiffener. Recently, Hayman *et al*. (2011) experimentally analyzed the ultimate strength of rectangular composite plates with geometrical imperfection under in-plane load. They validated their results with nonlinear finite element analysis. In addition, Yang *et al*. (2013) investigated the ultimate strength of composite plates with initial geometrical imperfections under in-plane compressive load through analyzing based on the first order shear deformation theory and regarding the assumptions of small deflection theory by using the Ritz method. The degradation model in their analysis was instantaneous material degradation which was applied in complete ply or region of failed ply. Further, in another similar study, Yang and Hayman (2015a) reported the same results based on the assumptions of large deflection theory. Furthermore, they evaluated the ultimate strength and geometric nonlinear behavior of composite laminated plates with initial geometric imperfections by adopting the linear material degradation model (Yang and Hayman 2015b). Recently, Ghannadpour and his co-workers focused on the geometric nonlinear and progressive damage behavior of relatively thick laminated flat plates under lateral pressure and end-shortening by using the Ritz method (Ghannadpour *et al*. 2018a). Ghannadpour and Shakeri (2018) introduced a new collocation methodology to predict failure and progressive damage behavior of composite plates under uniaxial in-plane compressive load. Ghannadpour *et al*. (2018b) presented two different computational methods, called Rayleigh-Ritz and collocation, to estimate the ultimate strength of moderately thick composite plates under in-plane compressive load and uniform lateral pressure.

In the present paper, ultimate strength, post-buckling and geometric nonlinear analysis of imperfect composite laminated plates are investigated using the Ritz method. In this regard, the imperfect composite plates are assumed to be subjected to both lateral pressure loading and end compression very similar to the panel structures of wing of aircrafts under lift forces. The out-of-plane boundary conditions are simply-supported and the first-order shear deformation theory is considered with the assumption of large deflections. The formulations are based on the concept of the principle of minimum potential energy. To solve the nonlinear set of algebraic equations, Newton–Raphson technique is used. In order to degrade the material properties, two geometric models such as degrading the material in the regions of the plies or degrading the entire plies are considered to estimate the degradation zone around the failure location. Further, the plates involving a range of thicknesses and geometric initial imperfection with different magnitudes of pressure loads are analyzed. Finally, how the ultimate strength of the imperfect composite plates can be changed in terms of the earlier mentioned parameters, will be discussed.

2. Theoretical development

In this study, ultimate strength of imperfect simply supported square composite plates with dimensions $a \times a$ and thickness h have been studied while they are subjected to both end-shortening strain e and lateral pressure loading P. The assumed shape of the initial geometric imperfection is a single half sine wave in each direction. In the current approach, the first order shear deformation plate theory is considered with the assumption of large deflections. According to these assumptions, the total potential energy of a laminate can be obtained. At first, the strain energy associated with the in-plane stresses can be written as

$$U_m = \frac{1}{2}\int_V \varepsilon^T \sigma \, dV = \frac{1}{2}\int_A \int_{-\frac{h}{2}}^{\frac{h}{2}} \varepsilon^T \bar{Q} \varepsilon \, dz \, dA \tag{1}$$

Where $\bar{Q}$ is transformed reduced stiffness matrix which is defined later and ε is the strain vector of the plate that can be written as

$$\varepsilon = \begin{Bmatrix} \varepsilon_{xx} \\ \varepsilon_{yy} \\ \varepsilon_{xy} \end{Bmatrix} = \varepsilon^0 + z\psi \tag{2a}$$

$$\varepsilon^0 = \begin{Bmatrix} \varepsilon_{xx}^0 \\ \varepsilon_{yy}^0 \\ \varepsilon_{xy}^0 \end{Bmatrix} = \varepsilon_l + \varepsilon_{nl} + \varepsilon_i + \varepsilon_e \tag{2b}$$

In the above relation, $\varepsilon_l, \varepsilon_{nl}, \varepsilon_i, \varepsilon_e$ are linear strains vector, nonlinear strains vector, strain vector for initial geometric imperfection and applied end-shortening strains vector, respectively and vector ψ is curvature strains vector of the plate. They can be defined as

$$\varepsilon_l = \begin{Bmatrix} \dfrac{\partial u}{\partial x} \\ \dfrac{\partial v}{\partial y} \\ \dfrac{\partial u}{\partial y} + \dfrac{\partial v}{\partial x} \end{Bmatrix}, \quad \varepsilon_i = \begin{Bmatrix} \dfrac{\partial w}{\partial x}\dfrac{\partial w_i}{\partial x} \\ \dfrac{\partial w}{\partial y}\dfrac{\partial w_i}{\partial y} \\ \dfrac{\partial w}{\partial x}\dfrac{\partial w_i}{\partial y} + \dfrac{\partial w}{\partial y}\dfrac{\partial w_i}{\partial x} \end{Bmatrix} \tag{3a}$$

$$\varepsilon_{nl} = \begin{Bmatrix} \dfrac{1}{2}\left(\dfrac{\partial w}{\partial x}\right)^2 \\ \dfrac{1}{2}\left(\dfrac{\partial w}{\partial y}\right)^2 \\ \dfrac{\partial w}{\partial x}\dfrac{\partial w}{\partial y} \end{Bmatrix}, \varepsilon_e = \begin{Bmatrix} -e \\ \alpha e \\ 0 \end{Bmatrix}, \quad \psi = \begin{Bmatrix} \dfrac{\partial \varphi_x}{\partial x} \\ \dfrac{\partial \varphi_y}{\partial y} \\ \dfrac{\partial \varphi_x}{\partial y} + \dfrac{\partial \varphi_y}{\partial x} \end{Bmatrix} \tag{3b}$$

Where parameter α indicates the Poisson effect and will be defined later. With these definitions, the strain energy can be re-written as

$$U_m = \frac{1}{2}\int_A \int_{-\frac{h}{2}}^{\frac{h}{2}} (\varepsilon_l + \varepsilon_{nl} + \varepsilon_i + \varepsilon_e + z\psi)^T \bar{Q} \, (\varepsilon_l + \varepsilon_{nl} + \varepsilon_i + \varepsilon_e + z\psi) \, dz dA \tag{4}$$

With the assumption that each layer is in a condition of plane stress, stress-strain relationship for each lamina at a general point is written as below

$$\sigma = \begin{Bmatrix} \sigma_{xx} \\ \sigma_{yy} \\ \tau_{xy} \end{Bmatrix} = \begin{bmatrix} \bar{Q}_{11} & \bar{Q}_{12} & \bar{Q}_{16} \\ \bar{Q}_{12} & \bar{Q}_{22} & \bar{Q}_{26} \\ \bar{Q}_{16} & \bar{Q}_{26} & \bar{Q}_{66} \end{bmatrix} \begin{Bmatrix} \varepsilon_{xx} \\ \varepsilon_{yy} \\ \gamma_{xy} \end{Bmatrix} \tag{5a}$$

$$\sigma_s = \bar{Q}_s \varepsilon_s = \begin{bmatrix} \bar{Q}_{44} & \bar{Q}_{45} \\ \bar{Q}_{45} & \bar{Q}_{55} \end{bmatrix} \begin{bmatrix} \varphi_y + \dfrac{\partial w}{\partial y} \\ \varphi_x + \dfrac{\partial w}{\partial x} \end{bmatrix} \tag{5b}$$

Where $\bar{Q}_{ij}(i,j = 1,2,6)$ are transformed reduced stiffness coefficients, $\bar{Q}_s$ is transformed shear stiffness matrix and the vector ε_s is the shear strains vector of the plate. Each composite plate has its stiffness matrices that their coefficients can be obtained by

$$\left(A_{ij}, B_{ij}, D_{ij}\right) = \int_{-\frac{h}{2}}^{\frac{h}{2}} \bar{Q}_{ij} \, (1, z, z^2) dz, \ \ i,j = 1,2,6 \tag{6a}$$

$$A_{ij} = \int_{-\frac{h}{2}}^{\frac{h}{2}} \bar{Q}_{ij} \, dz, \ \ i,j = 4,5 \tag{6b}$$

With integrating through the thickness with respect to z from Eq. (4) and substituting Eq. (6) into Eq. (4), the strain energy associated with the in-plane stresses can be rewritten as

$$\begin{aligned} U_m = & \int_A \frac{1}{2}\varepsilon_e^T A \varepsilon_e dA \\ & + \int_A (\varepsilon_l^T A \varepsilon_e + \varepsilon_i^T A \varepsilon_e + \psi^T B \varepsilon_e) dA \\ & + \int_A (\frac{1}{2}\varepsilon_l^T A \varepsilon_l + \varepsilon_l^T A \varepsilon_i + \varepsilon_l^T B \psi + \frac{1}{2}\varepsilon_i^T A \varepsilon_i \\ & + \varepsilon_i^T B \psi + \frac{1}{2}\psi^T D \psi + \varepsilon_{nl}^T A \varepsilon_e) dA \\ & + \int_A (\varepsilon_l^T A \varepsilon_{nl} + \varepsilon_{nl}^T A \varepsilon_i + \varepsilon_{nl}^T B \psi) dA \\ & + \int_A \frac{1}{2}\varepsilon_{nl}^T A \varepsilon_{nl} dA \end{aligned} \tag{7}$$

In the above expression there is a clear division, indicated by the five integrals, into five categories of strain energy U_m. The first term in right-hand side of the above equation is independent of the unknowns and therefore has no effect in minimizing the total potential energy while the rest of terms are linear, quadratic, cubic and quartic functions of the unknowns, respectively.

In the next step, shear strain energy U_s should be computed that can be obtained by the following relation.

$$\begin{aligned} U_s &= \frac{1}{2}k_s \int_V \varepsilon_s^T \sigma_s dV = \frac{1}{2}k_s \int_A \int_{-\frac{h}{2}}^{\frac{h}{2}} \varepsilon_s^T \bar{Q}_s \varepsilon_s \ dz dA \\ &= \frac{1}{2}k_s \int_A \left(A_{44}\left(\varphi_y + \frac{\partial w}{\partial y}\right)^2 \right. \end{aligned} \tag{8}$$

$$+2A_{45}\left(\varphi_y+\frac{\partial w}{\partial y}\right)\left(\varphi_x+\frac{\partial w}{\partial x}\right)$$
$$+A_{55}\left(\varphi_x+\frac{\partial w}{\partial x}\right)^2\Bigg)dA \tag{8}$$

Where k_s is the shear correction factor and it is assumed to be equal to 5/6 in this study. Since, the lateral pressure load $P(x,y)$ is applied on the whole plate therefore; the external load exists in the current problem. As a result, the total potential energy is equal to the summation of strain energies and potential energy of the lateral pressure load. The potential energy of the external load U_P is given by

$$U_P=-\int_A P(x,y)w\,dA \tag{9}$$

It is noted that uniform lateral pressure distribution have been assumed to be applied on the plates (i.e., $P(x,y)=p_0$). With the above descriptions, the total potential energy is equal to

$$\Pi=U_m+U_s+U_P \tag{10}$$

Nonlinear responses can be found by solution of the nonlinear algebraic equations obtained through the application of the principle of minimum potential energy. To obtain the solution of the aforementioned nonlinear algebraic equations, the well-known Newton–Raphson technique is used here.

3. Boundary conditions and displacement fields

As mentioned earlier, the simply supported square composite plates have been subjected to end-shortening strain e and lateral pressure loading. This is attained by restraining the edge $x=0$ in the *x*-direction and applying a uniform and negative displacement $u=-ea$ in the *x*-direction on the edge $x=a$ as represented in Fig. 1. The lower and left edges of the laminates are restricted from any movement and the two others can move straightly. These boundary conditions are also represented in Fig. 1.

According to the above mentioned boundary conditions, the required displacement fields can be written as

$$\varphi_x(x,y)=\sum_{n=1}^{n_t}\sum_{m=1}^{n_t}X_{mn}\cos\left(\frac{m\pi x}{a}\right)\sin\left(\frac{n\pi y}{a}\right) \tag{11a}$$

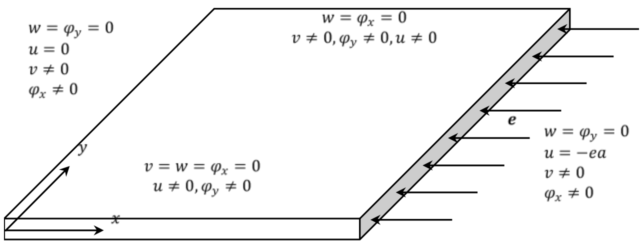

Fig. 1 Plates boundary conditions

$$\varphi_y(x,y)=\sum_{n=1}^{n_t}\sum_{m=1}^{n_t}Y_{mn}\sin\left(\frac{m\pi x}{a}\right)\cos\left(\frac{n\pi y}{a}\right) \tag{11b}$$

$$w(x,y)=\sum_{n=1}^{n_t}\sum_{m=1}^{n_t}w_{mn}\sin\left(\frac{m\pi x}{a}\right)\sin\left(\frac{n\pi y}{a}\right)+\bar{w}_i\sin\left(\frac{\pi x}{a}\right)\sin\left(\frac{\pi y}{a}\right) \tag{11c}$$

$$u(x,y)=\sum_{n=1}^{n_t}\sum_{m=1}^{n_t}u_{mn}\sin\left(\frac{m\pi x}{a}\right)\sin\left(\frac{n\pi y}{a}\right) \tag{11d}$$

$$v(x,y)=\sum_{n=1}^{n_t}\sum_{m=1}^{n_t}v_{mn}\sin\left(\frac{m\pi x}{a}\right)\sin\left(\frac{n\pi y}{a}\right)+\frac{v_c y}{a} \tag{11e}$$

The coefficients $u_{mn},v_{mn},v_c,X_{mn},Y_{mn}$ and w_{mn} are unknown parameters, $\bar{w}_i$ is given imperfection amplitude, m and n are positive integers and n_t is the number of terms in each of displacement fields and for both x and y directions. The last term in the displacement field v is for satisfaction of the straight conditions of two adjacent edges. In order to satisfy the condition $u=-ea$ on the edge $x=a$, the term $-ex$ should be included in the displacement field u. Also, the term αey should be added to the displacement field v to show the Poisson effect of the applied end-shortening in which the parameter α can be approximated by A_{12}/A_{22} for composite materials. The effects of these terms can be observed in the strain vectors which were represented by Eq. (3).

Once the unknown parameters are found for a prescribed end-shortening strain using the mentioned procedure in section 2, it is possible to compute the displacement at any point in each lamina using Eq. (11). In order to determine the forces acting on a plate, the constitutive equations should be obtained. They can be calculated through use of Eqs. (2), (3), (5) and (6) and appropriate integration through the thickness.

$$\begin{Bmatrix}N_x\\N_y\\N_{xy}\end{Bmatrix}=\begin{bmatrix}A_{11}&A_{12}&A_{16}\\A_{12}&A_{22}&A_{26}\\A_{16}&A_{26}&A_{66}\end{bmatrix}\begin{Bmatrix}\varepsilon_{xx}^0\\\varepsilon_{yy}^0\\\varepsilon_{xy}^0\end{Bmatrix}+\begin{bmatrix}B_{11}&B_{12}&B_{16}\\B_{12}&B_{22}&B_{26}\\B_{16}&B_{26}&B_{66}\end{bmatrix}\begin{Bmatrix}\psi_x\\\psi_y\\\psi_{xy}\end{Bmatrix} \tag{12a}$$

$$\begin{Bmatrix}M_x\\M_y\\M_{xy}\end{Bmatrix}=\begin{bmatrix}B_{11}&B_{12}&B_{16}\\B_{12}&B_{22}&B_{26}\\B_{16}&B_{26}&B_{66}\end{bmatrix}\begin{Bmatrix}\varepsilon_{xx}^0\\\varepsilon_{yy}^0\\\varepsilon_{xy}^0\end{Bmatrix}+\begin{bmatrix}D_{11}&D_{12}&D_{16}\\D_{12}&D_{22}&D_{26}\\D_{16}&D_{26}&D_{66}\end{bmatrix}\begin{Bmatrix}\psi_x\\\psi_y\\\psi_{xy}\end{Bmatrix} \tag{12b}$$

The average longitudinal force N_{av} can be computed by integrating the membrane stress resultant N_x over the plate area as follows

$$N_{av} = \frac{\int_0^a \int_0^a N_x(x,y)dxdy}{a} \tag{13}$$

4. Hashin and Rotem failure criteria

The failure criteria adopted in this study have been reported by Hashin and Rotem (1973). These criteria are corresponding to the different modes of failure namely fiber tension, fiber compression, matrix tension, and matrix compression.

$Fiber\ failure\ in\ tension$:

$$\left(\frac{\sigma_1}{X_t}\right)^2 = 1 \tag{14a}$$

$Fiber\ failure\ in\ compression$:

$$\left(\frac{\sigma_1}{X_c}\right)^2 = 1 \tag{14b}$$

$Matrix\ failure\ in\ tension$:

$$\left(\frac{\sigma_2}{Y_t}\right)^2 + \left(\frac{\tau_{12}}{S_{12}}\right)^2 = 1 \tag{14c}$$

$Matrix\ failure\ in\ compression$:

$$\left(\frac{\sigma_2}{Y_c}\right)^2 + \left(\frac{\tau_{12}}{S_{12}}\right)^2 = 1 \tag{14d}$$

Where parameters X_t, X_c, Y_t, Y_c and S_{12} indicate the ultimate tensile strength of fiber, ultimate compression strength of fiber, ultimate tensile strength of matrix, ultimate compression strength of matrix and ultimate shear strength, respectively. The stresses in each layer may be computed by Eq. (5). Satisfaction of just one of these criteria is enough to predict the failure.

5. Degradation of material properties

In this study, two different degradation models are applied whenever failure is predicted in a laminate. These models are complete ply degradation and ply region degradation models. If the degradation of property is applied to the entire ply, the model is complete ply degradation model while in the ply region degradation model, each ply is divided in to nine regions and the stiffness of the predicted region is reduced (see Fig. 2).

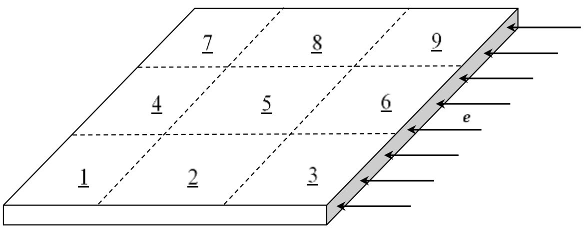

Fig. 2 A typical laminate with nine regions

This degradation can be implemented by the following damaged stiffness matrix

$$R = \begin{bmatrix} (1-d_1)R_{11} & (1-d_1)(1-d_2)R_{12} & 0 \\ sym & (1-d_2)R_{22} & 0 \\ sym & sym & R_{66} \end{bmatrix} \tag{15}$$

Where

$$R_{11} = \frac{E_1}{1-\vartheta_{12}\vartheta_{21}(1-d_1)(1-d_2)} \tag{16a}$$

$$R_{12} = \frac{\vartheta_{12}E_2}{1-\vartheta_{12}\vartheta_{21}(1-d_1)(1-d_2)} \tag{16b}$$

$$R_{22} = \frac{E_2}{1-\vartheta_{12}\vartheta_{21}(1-d_1)(1-d_2)} \tag{16c}$$

$$R_{66} = (1-d_1)(1-d_2)G_{12} \tag{16d}$$

Here d_1 and d_2 are damage factors in the longitudinal and transverse directions of the material, respectively. In this research, the degradation of material properties is assumed to be instantaneously and to 1% of the initial value for failed ply or region of failed ply. It should be noted that in this paper, it is assumed that the failure does not occur between the layers and therefore the shear stiffness matrix does not change during the analysis.

6. Results and discussions

The square laminated plates with dimensions $a \times a\ (a = 500\ mm)$ with layup configuration $[0/45/90/-45]_{X,s}$ are investigated here. The thickness of each layer is assumed to be 1 mm and X gets the values of 1, 3 and 6. Each lamina has material properties of $E_1 = 49627$ MPa, $E_2 = 15430$ MPa, $\vartheta_{12} = 0.272$, $G_{12} = G_{23} = G_{13} = 4800$ MPa, $X_t = 968$ MPa, $X_c = 915$ MPa, $Y_t = 24$ MPa, $Y_c = 118$ MPa and $S_{12} = 65$ MPa. As mentioned before, uniform lateral pressure load is also applied on the plates $P(x,y) = p_0$. In order to show the results, a pressure load

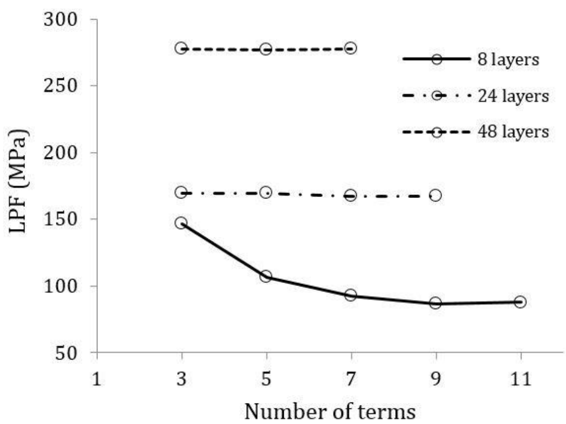

Fig. 3 Convergence study of the square laminates under uniform lateral pressure ($Q = 2$)

Table 1 Complete ply degradation results under uniform lateral pressure (in MPa)

X	$\bar{w}_i$ (mm)	Q	FPF	(1)	LPF	(1)	(2)	(3)
1	0	0	29.27	8 (250,250)	88.17	7 (10,0)	8	1
		1	24.62	8 (250,250)	87.26	7 (10,0)	8	1
		2	20.18	8 (250,250)	86.46	7 (10,0)	8	1
		3	15.95	8 (250,270)	85.58	2 (0,500)	8	2
		6.9194	0	8 (240,170)	82.52	2 (0,500)	8	2
	5	0	27.18	8 (260,330)	89.87	2 (0,500)	8	2
		1	24.20	8 (240,160)	89.13	2 (0,500)	8	2
		2	21.16	8 (260,360)	88.36	2 (0,500)	8	2
		3	17.91	8 (260,370)	87.78	2 (0,500)	8	2
		8.4112	0	8 (260,390)	83.87	2 (0,500)	8	2
	15	0	26.02	8 (250,100)	93.39	7 (10,0)	8	1
		1	24.04	8 (250,400)	92.37	7 (10,0)	8	1
		2	21.84	8 (250,410)	91.60	7 (10,0)	8	1
		3	19.61	8 (250,410)	90.99	7 (10,0)	8	1
		11.6570	0	8 (250, 80)	86.46	1 (40,30)	8	2
3	0	0	205.23	22 (250,250)	205.23	22 (250,250)	1	0
		1	143.62	24 (250,250)	172.58	23 (0,0)	24	1
		2	93.58	24 (250,250)	167.22	23 (0,0)	24	1
		3	50.25	24 (250,250)	162.25	2 (0,500)	24	2
		4.3417	0	24 (250,250)	155.25	2 (0,500)	24	2
	5	0	67.89	24 (250,250)	169.97	2 (0,500)	24	2
		1	51.48	24 (250,250)	165.35	2 (0,500)	24	2
		2	35.26	24 (250,250)	160.47	2 (0,500)	24	2
		3	19.73	24 (250,250)	155.84	2 (0,500)	24	2
		4.3065	0	24 (250,250)	149.55	2 (0,500)	24	2
	15	0	35.17	24 (250,250)	159.40	2 (0,500)	24	2
		1	28.14	24 (250,250)	155.49	2 (0,500)	24	2
		2	21.25	24 (250,250)	151.52	2 (0,500)	24	2
		3	14.54	24 (250,250)	147.47	2 (0,500)	24	2
		5.1106	0	24 (250,330)	138.97	2 (0,500)	24	2
6	0	0	209.38	3 (0,0)	309.04	48 (470,180)	48	0
		1	196.35	3 (250,250)	290.72	1 (250,250)	40	1
		2	184.62	3 (250,250)	277.70	1 (250,250)	41	1
		3	117.10	48 (250,250)	263.94	1 (250,250)	42	1
		4.2002	0	48 (250,250)	249.93	1 (250,250)	42	1
	5	0	142.69	48 (250,250)	249.46	1 (250,250)	42	1
		1	106.27	48 (250,250)	240.90	1 (250,250)	42	1
		2	70.97	48 (250,250)	232.81	1 (250,250)	42	1
		3	36.97	48 (250,250)	225.96	1 (250,250)	42	1
		4.0862	0	48 (250,250)	217.44	1 (250,250)	42	1
	15	0	61.16	48 (250,250)	209.97	1 (250,230)	48	1
		1	46.12	48 (250,250)	205.49	1 (250,230)	48	1
		2	31.43	48 (250,250)	201.41	1 (250,220)	48	1
		3	16.60	48 (250,250)	197.70	1 (250,220)	48	1
		4.1240	0	48 (250,250)	192.78	1 (240,210)	48	1

(1) Ply No. (coordinates of failure); (2) No. of plies with failed matrix; (3) No. of plies with failed fiber;
FPF: First Ply Failure stress; LPF: Last Ply Failure stress

factor is defined as $Q = np_0a^3/8D_{22}$ where n is the number of layers in the laminates and p_0 is the magnitude of applied pressure load.

A convergence test is performed to find the sufficient number of terms in the displacement fields for the laminates with different number of layers. To do this, a convergence study is conducted to find the ultimate strength or Last Ply Failure (LPF) stress of square laminates with $X = 1, 3$ and 6. In these laminates, uniform lateral pressure load $Q = 2$ is applied.

As shown in Fig. 3, the convergent results for thinner plates are obtained by higher number of terms while considerably lower number of terms are required for laminates having thicker thickness. Thus, in this paper, the number of terms is assumed to be 9 ($n_t = 9$) for thin plates with $X = 1$, upon which the total number of unknown coefficients for this number of terms is 406 and the number of terms are taken to be 7 in each displacement field for the thick laminates with $X = 3$ and 6. Therefore, the total number of unknown coefficients is 246 for these types of laminates.

The progressive damage results for complete ply degradation model and for laminates subjected to uniform lateral pressure load are tabulated in Table 1. These results have been computed for laminates with 8, 24 and 48 mm thicknesses and therefore all results have been presented for 5 different values of lateral pressure load factors. The magnitude of load factors is selected to be $Q = 0, 1, 2, 3, Q_s$. The parameter Q_s is considered as a specific load factor in which the first ply failure (FPF) occurs in zero applied longitudinal stress. As shown, this table includes the calculated first ply failure stress and location of the failure in terms of ply number and coordinates of the failure point. Further, the ultimate strength or last ply failure (LPF) stress, the failure location (i.e., ply number and coordinates of failure point), as well as the number of layers whose matrix or fiber fails are displayed in Table 1.

As shown, the first ply failure stress and ultimate strength increase by increasing the number of layers while they decrease by increasing the magnitude of imperfection, except for the plates with lower thickness. All results tabulated in the table above are presented in Figs. 4 to 21 to

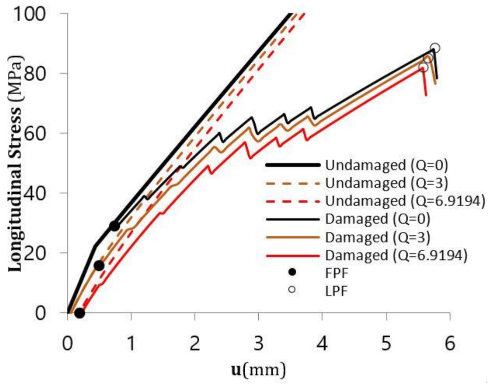

Fig. 4 Load-end displacement behavior for 8-layer laminate without imperfection under end-shortening and uniform pressure loading using complete ply degradation model

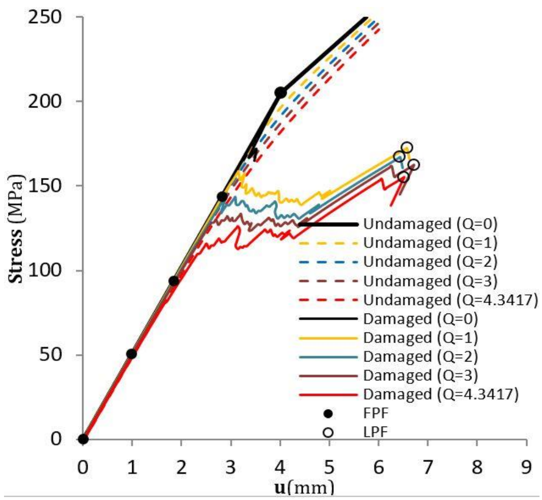

Fig. 6 Load-end displacement behavior for 24-layer laminate under end-shortening and uniform pressure loading using complete ply degradation model

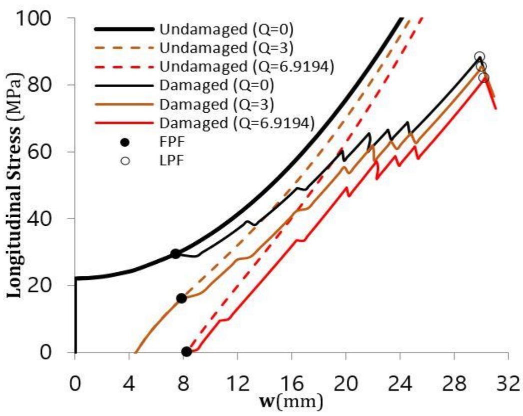

Fig. 5 Load-deflection behavior for 8-layer laminate under end-shortening and uniform pressure loading using complete ply degradation model

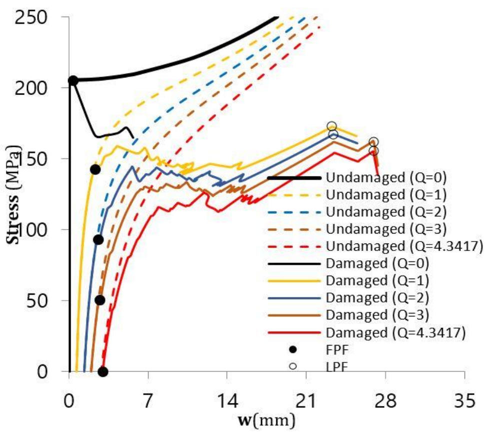

Fig. 7 Load-deflection behavior for 24-layer laminate under end-shortening and uniform pressure loading using complete ply degradation model

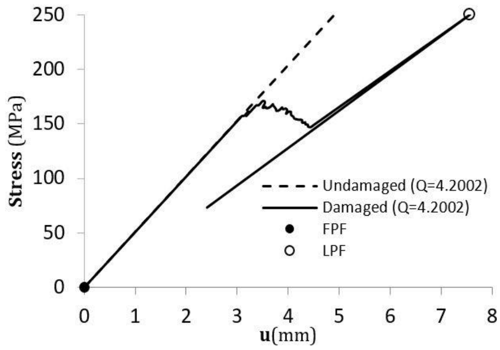

Fig. 8 Load-end displacement behavior for 48-layer laminate under end-shortening and uniform pressure loading using complete ply degradation model

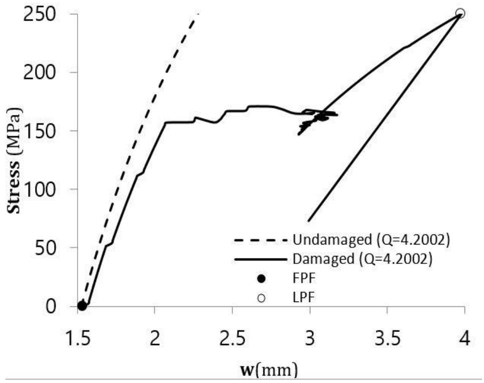

Fig. 9 Load-deflection behavior for 48-layer laminate under end-shortening and uniform pressure loading using complete ply degradation model

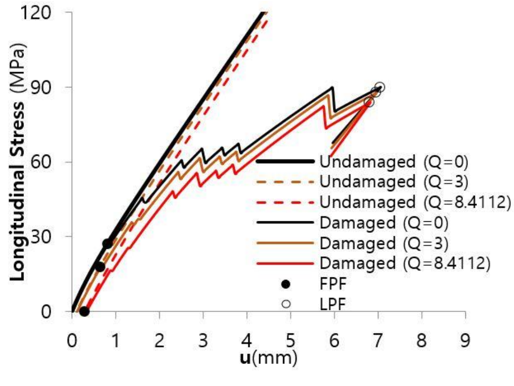

Fig. 10 Load-end displacement behavior for 8-layer laminate with imperfection 5 mm under end-shortening and uniform pressure loading using complete ply degradation model

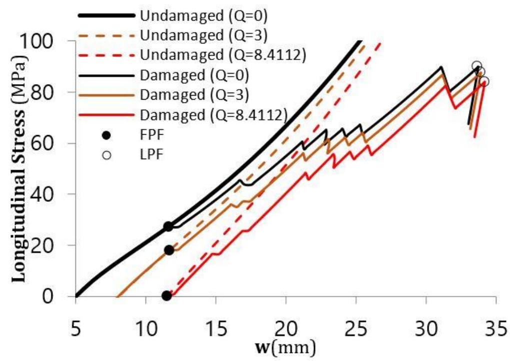

Fig. 11 Load-deflection behavior for 8-layer laminate with imperfection 5 mm under end-shortening and uniform pressure loading using complete ply degradation model

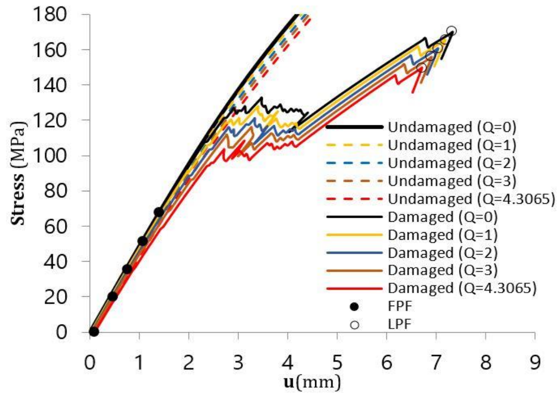

Fig. 12 Load-end displacement behavior for 24-layer laminate with imperfection 5 mm under end-shortening and uniform pressure loading using complete ply degradation model

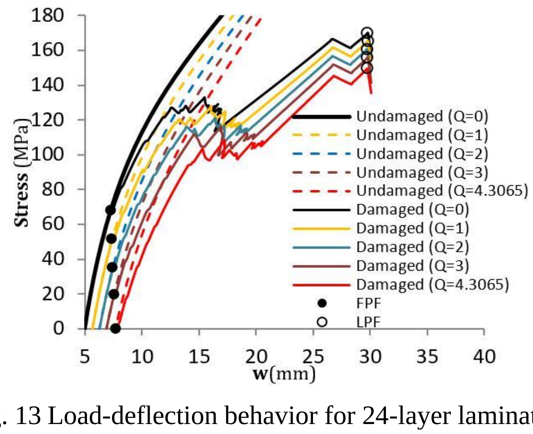

Fig. 13 Load-deflection behavior for 24-layer laminate with imperfection 5 mm under end-shortening and uniform pressure loading using complete ply degradation model

illustrate the behavior of load in terms of end-longitudinal displacement and versus central out-of-plane displacement. To illustrate the differences between the two analyzes with the assumption of damage and without damage, the results of both analyzes are presented in these figures. The first and last ply failure stresses are marked with solid and hollow circles, respectively. Based on the results, the last and first ply failure stresses decrease by increasing the load factor Q while the reduction rate in the last ply failure stress is

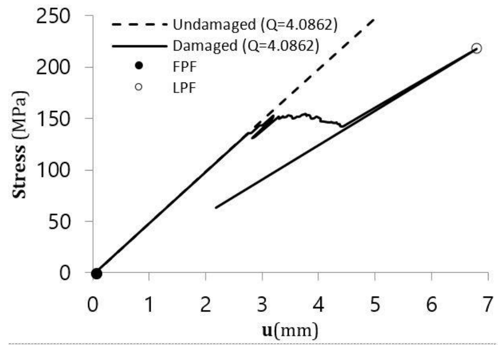

Fig. 14 Load-end displacement behavior for 48-layer laminate with imperfection 5 mm under end-shortening and uniform pressure loading using complete ply degradation model

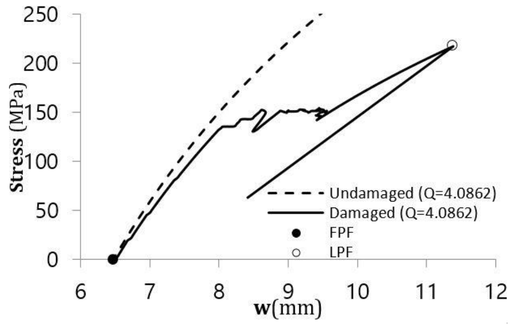

Fig. 15 Load-deflection behavior for 48-layer laminate with imperfection 5 mm under end-shortening and uniform pressure loading using complete ply degradation model

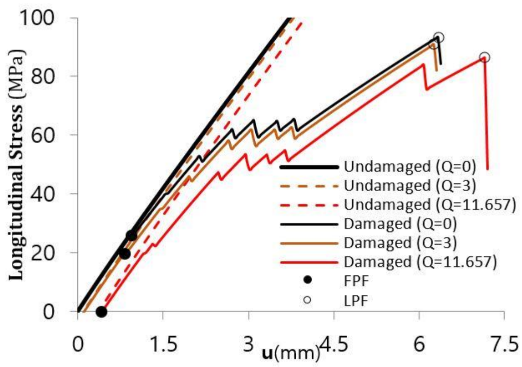

Fig. 16 Load-end displacement behavior for 8-layer laminate with imperfection 15 mm under end-shortening and uniform pressure loading using complete ply degradation model

considerably lower than the first ply failure load. As mentioned earlier, the undamaged results are also depicted in these figures. As it is seen, both series of the results are distinct from each other at the beginning while they get closer at the end. In addition, as shown in Table 1, the first ply failure almost occurs in the center of the last layer. Further, the ultimate load is associated with the fiber failure

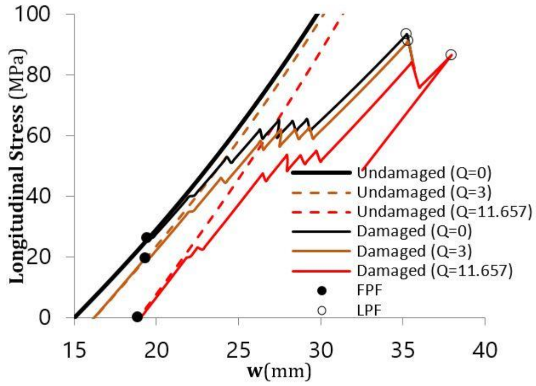

Fig. 17 Load-deflection behavior for 8-layer laminate with imperfection 15 mm under end-shortening and uniform pressure loading using complete ply degradation model

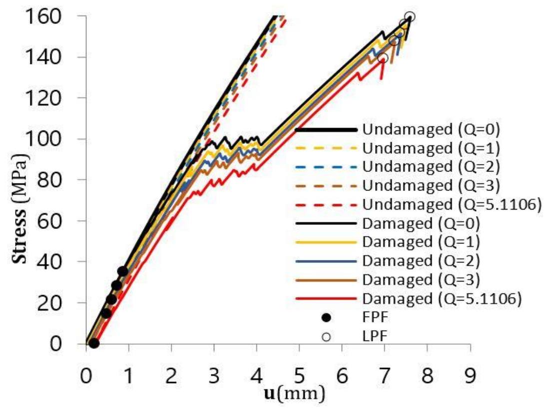

Fig. 18 Load-end displacement behavior for 24-layer laminate with imperfection 15 mm under end-shortening and uniform pressure loading using complete ply degradation model

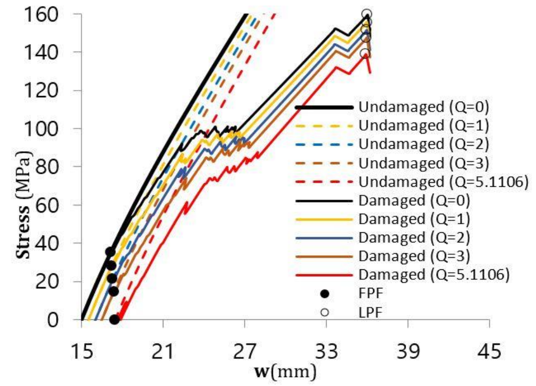

Fig. 19 Load-deflection behavior for 24-layer laminate with imperfection 15 mm under end-shortening and uniform pressure loading using complete ply degradation model

in most cases. Based on the observations, the failure for 0^o and 90^o plies often occurs first in the center of the plate, while the $\pm 45^0$ plies fail at the corners. Furthermore, the last ply failure occurred more in the corners of the plates in the plate with lower thickness (the plates with thicknesses 8 and 24 mm) and the last ply failure happened in the center of plate in the laminates with higher thickness. It was also seen that the first ply failure for most of the plates occurred as matrix failure in the center of the outermost 0° plies on the convex side of the plate for all cases except for the thickest plates with lower pressure load factor. Regarding the layup, the first ply failure occurred in the 90° ply.

As illustrated in these figures, the laminates have the same load-displacement behaviors under different load factors. Additionally, the center deflection increases by enhancing load factor Q, and the plates do not have buckling point without imperfection under lateral pressure. Accordingly, the plate is deflected from the start of loading.

In addition, regarding the plates without imperfection, the first ply failures occur considerably earlier than those in the thin laminates by increasing the thickness of the laminates. In other words, the plates with lower thickness are more prone to enter into the post-buckling regime or nonlinear region. Of course, it is obvious that the thick laminates have considerably higher first ply failure loads than those for thin laminates although these loads are often happened in the linear region.

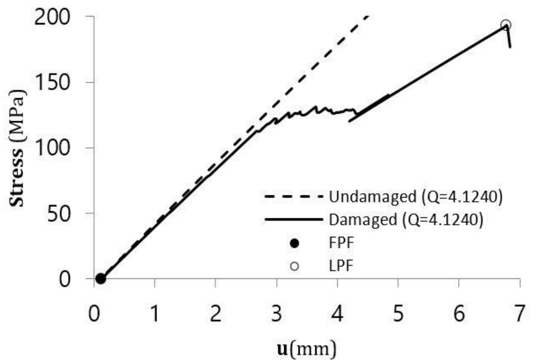

Fig. 20 Load-end displacement behavior for 48-layer laminate with imperfection 15 mm under end-shortening and uniform pressure loading using complete ply degradation model

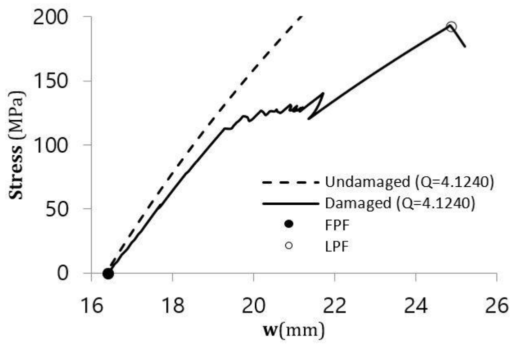

Fig. 21 Load-deflection behavior for 48-layer laminate with imperfection 15 mm under end-shortening and uniform pressure loading using complete ply degradation model

Further, it is seen that the effects of lateral pressure loading and initial imperfection are separately similar and therefore the laminates with different magnitudes of imperfection or under different pressure load factors have the same load-displacement behaviors along their loading paths. Furthermore, the plates involving imperfection do not have buckling point and they are deflected from the start ofloading and entered into the nonlinear region.

Based on the Figs. 14 and 15, it is observed that the longitudinal stress for the laminate with 48 layers drops sharply after reaching the last ply failure load and this reduction mostly occurs after a fiber failure in a lamina.

According to these observations, the first and last ply failure loads decrease by increasing the magnitude of imperfection or values of lateral pressure load.

Table 3 presents the progressive damage results for the laminates by using ply region degradation model under uniform lateral pressure load. To apply the ply region degradation model, it is necessary to define the size of the regions represented in Fig. 2. They can be found in the Table 2.

The results have been calculated for the laminates with 8, 24 and 48 mm thicknesses and for different magnitudes of imperfection 0, 5 and 15 mm and also for five different values of lateral pressure load factors $Q = 0, 1, 2, 3, Q_s$ same as in Table 1. Similar to the results based on complete ply degradation model, Table 3 involves the calculated stress at first ply failure, location of the failure, ultimate strength, and the number of regions whose matrix or fiber fails.

Based on the results in Tables 1 and 3 and as expected, no difference is observed between the first ply failure loads obtained by both complete ply degradation and ply region degradation models. However, the last ply failure in the ply region degradation model is slightly higher than that in the complete ply degradation model.

In ultimate strength analysis of the laminates with thicknesses of 24 and 48 mm under the uniform lateral pressure distribution with the same intensity, an increase in initial geometric imperfection reduces the first ply failure loads by 32-86%, as presented in Table 1. Regarding the thinner plates with a thickness of 8 mm under lateral pressure load, it decreases by 0.5-11% for pressure load factor $Q = 0, 1$ and increases by 3-23% for $Q = 2, 3$. Further, the ultimate load of the laminates having thicker thicknesses and same initial geometric imperfection (24 and 48 layers) with increases lateral pressure load factor, reduces by 8-24%, while the final strength of the thin plates with the thickness of 8 mm increases by 6-8%.

Table 2 Assumed sizes for regions in ply region degradation model

Region	Dimensions
1, 3, 7 and 9	$0.32a \times 0.32a$
2 and 8	$0.36a \times 0.32a$
4 and 6	$0.32a \times 0.36a$
5	$0.36a \times 0.36a$

Table 3 Ply region degradation results under uniform lateral pressure (in MPa)

X	$\bar{w}_i$ (mm)	Q	FPF	(1)	LPF	(2)	(3)
1	0	0	29.27	8(250,250)	105.33	59	4
		1	24.62	8(250,250)	104.75	59	4
		2	20.18	8(250,250)	104.04	59	4
		3	15.95	8(250,270)	103.89	59	4
		6.9194	0	8(240,170)	101.35	59	4
	5	0	27.18	8(260,330)	106.27	56	4
		1	24.20	8(240,160)	105.28	56	4
		2	21.16	8(260,360)	104.87	56	4
		3	17.91	8(260,370)	104.33	56	4
		8.4112	0	8(260,390)	101.10	56	4
	15	0	26.02	8(250,100)	104.02	54	4
		1	24.04	8(250,400)	103.16	54	4
		2	21.84	8(250,410)	102.69	54	4
		3	19.61	8(250,410)	102.21	54	4
		11.6570	0	8(250, 80)	100.77	56	4
3	0	0	205.23	22(250,250)	205.23	1	0
		1	143.62	24(250,250)	169.50	208	1
		2	93.58	24(250,250)	167.18	208	1
		3	50.25	24(250,250)	164.38	206	3
		4.3417	0	24(250,250)	163.06	204	3
	5	0	67.89	24(250,250)	173.99	208	4
		1	51.48	24(250,250)	172.16	208	4
		2	35.26	24(250,250)	170.03	206	4
		3	19.73	24(250,250)	167.95	206	4
		4.3065	0	24(250,250)	164.41	204	4
	15	0	35.17	24(250,250)	170.22	204	4
		1	28.14	24(250,250)	167.02	204	4
		2	21.25	24(250,250)	162.35	202	4
		3	14.54	24(250,250)	157.75	200	4
		5.1106	0	24(250,330)	150.13	200	4
6	0	0	209.38	3(0,0)	309.04	324	108
		1	196.35	3(250,250)	291.41	354	1
		2	184.62	3(250,250)	276.83	367	1
		3	117.10	48(250,250)	265.00	370	1
		4.2002	0	48(250,250)	249.98	374	1
	5	0	142.69	48(250,250)	249.46	378	1
		1	106.27	48(250,250)	240.90	378	1
		2	70.97	48(250,250)	233.62	378	1
		3	36.97	48(250,250)	225.96	378	1
		4.0862	0	48(250,250)	215.27	377	1
	15	0	61.16	48(250,250)	204.30	389	1
		1	46.12	48(250,250)	199.48	389	1
		2	31.43	48(250,250)	193.82	390	1
		3	16.60	48(250,250)	189.31	392	1
		4.1240	0	48(250,250)	183.92	394	1

(1) Ply No. (coordinates of first ply failure); (2) No. of regions with failed matrix; (3) No. of regions with failed fiber; FPF: First Ply Failure stress; LPF: Last Ply Failure stress

Like previous for the results of complete ply degrada- tion model, the loading paths for imperfect laminates involving the variation of load versus end longitudinal displacement and central out-of-plane displacement are depicted in Figs. 22-33 for some selected values in Table 3. The first and last ply failure stresses like the previous figures are marked with solid and hollow circles, respectively and undamaged results are also displayed in these figures in addition to the results based on the progressive damage analysis.

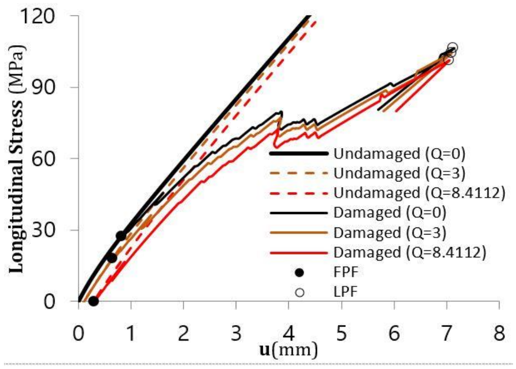

Fig. 22 Load-end displacement behavior for 8-layer laminate with imperfection 5 mm under end-shortening and uniform pressure loading using ply region degradation model

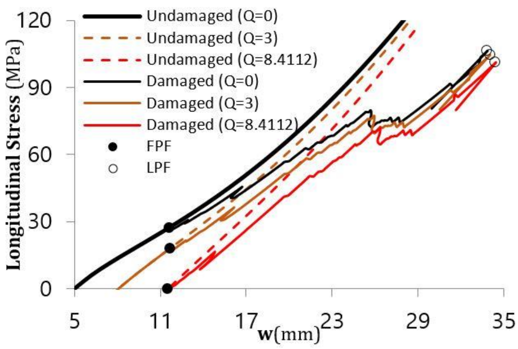

Fig. 23 Load-deflection behavior for 8-layer laminate with imperfection 5 mm under end-shortening and uniform pressure loading using ply region degradation model

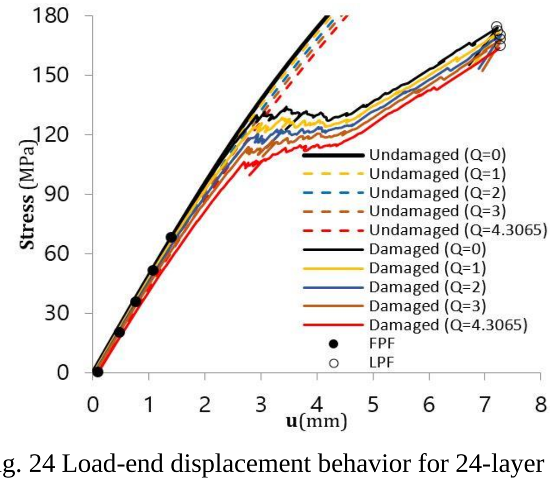

Fig. 24 Load-end displacement behavior for 24-layer laminate with imperfection 5 mm under end-shortening and uniform pressure loading using ply region degradation model

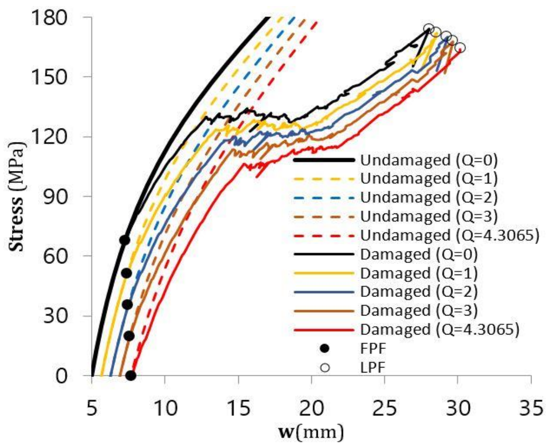

Fig. 25 Load-deflection behavior for 24-layer laminate with imperfection 5 mm under end-shortening and uniform pressure loading using ply region degradation model

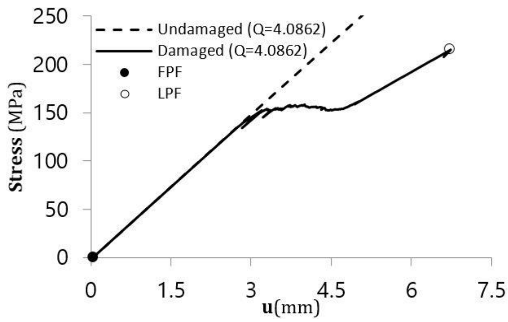

Fig. 26 Load-end displacement behavior for 48-layer laminate with imperfection 5 mm under end-shortening and uniform pressure loading using ply region degradation model

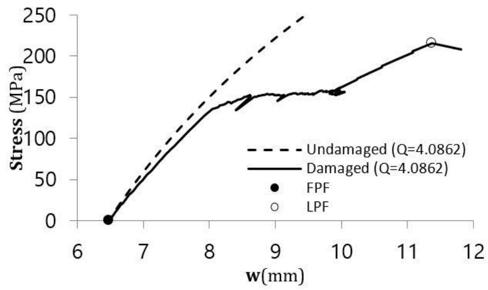

Fig. 27 Load-deflection behavior for 48-layer laminate with imperfection 5 mm under end-shortening and uniform pressure loading using ply region degradation model

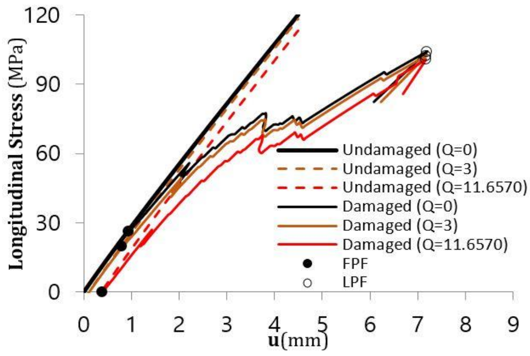

Fig. 28 Load-end displacement behavior for 8-layer laminate with imperfection 15 mm under end-shortening and uniform pressure loading using ply region degradation model

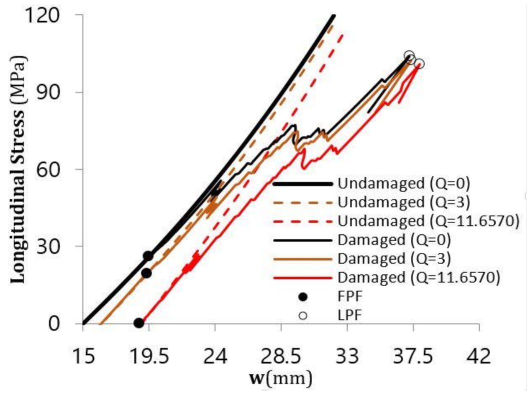

Fig. 29 Load-deflection behavior for 8-layer laminate with imperfection 15 mm under end-shortening and uniform pressure loading using ply region degradation model

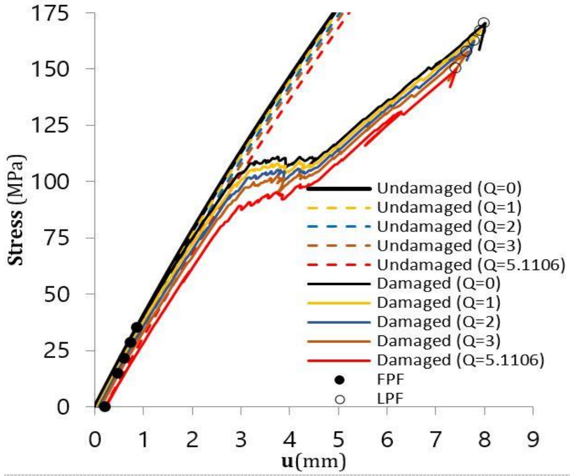

Fig. 30 Load-end displacement behavior for 24-layer laminate with imperfection 15 mm under end-shortening and uniform pressure loading using ply region degradation model

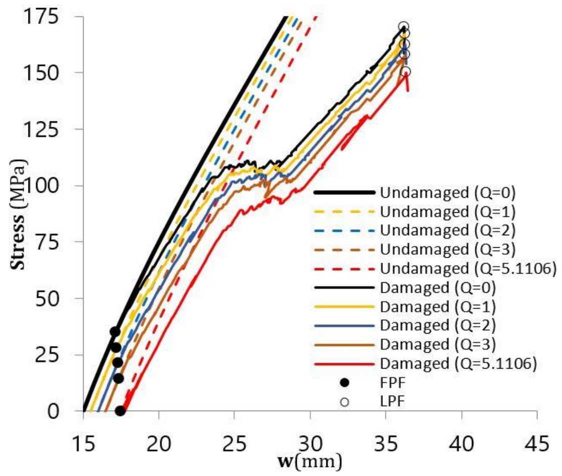

Fig. 31 Load-deflection behavior for 24-layer laminate with imperfection 15 mm under end-shortening and uniform pressure loading using ply region degradation model

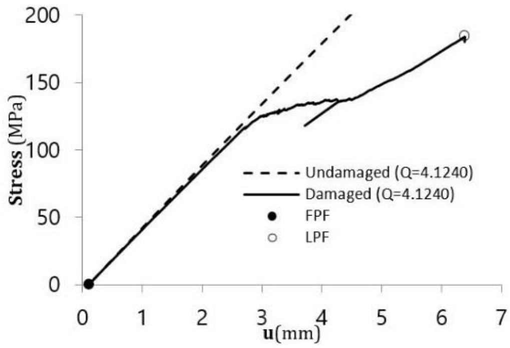

Fig. 32 Load-end displacement behavior for 48-layer laminate with imperfection 15 mm under end-shortening and uniform pressure loading using ply region degradation model

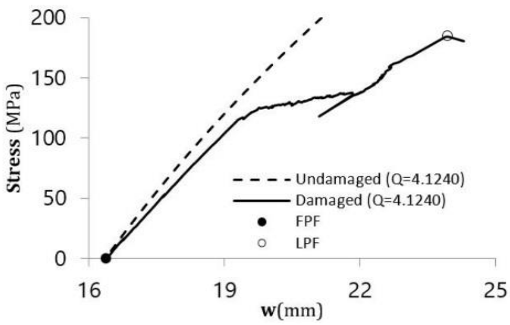

Fig. 33 Load-deflection behavior for 48-layer laminate with imperfection 15 mm under end-shortening and uniform pressure loading using ply region degradation model

7. Conclusions

The present study investigated the ultimate strength and post-buckling behavior of composite plates with simply supported boundary conditions under end-shortening and uniform lateral pressure loading, were assumed to be applied on the plates. The studied plates had different thicknesses and initial geometric imperfection. The analyses were performed using the Ritz method and the first order shear deformation theory. The displacement fields were estimated in the form of a double Fourier series. The convergence study was performed for the number of terms in the analysis and it was found that 49 and 81 terms are required to be used in each displacement field. The degradation of material properties was instantaneous after failure. Further, the Hashin and Rotem failure theory was used in failure analysis. Two models were investigated to reduce material degradation. The first one is the complete ply degradation model, in which the material properties of each layer decreases to 1% of the pre-failure state after failure, and the second is the ply region degradation model, in which each layer is divided into 9 regions, which only the properties of the failure-occurred area are degraded after failure.

References

Aghaei, M., Forouzan, M.R., Nikforouz, M. and Shahabi, E. (2015), “A study on different failure criteria to predict damage in glass/polyester composite beams under low velocity impact”, *Steel Compos. Struct., Int. J.*, **18**(5), 1291-1303. https://doi.org/10.12989/scs.2015.18.5.1291

Argyris, J. and Tenek, L. (1997), “Recent advances in computational thermostructural analysis of composite plates and shells with strong nonlinearities”, *Appl. Mech. Rev.*, **50**(5), 285-306. https://doi.org/10.1115/1.3101708

Becheri, T., Amara, K., Bouazza, M. and Benseddiq, N. (2016), “Buckling of symmetrically laminated plates using n^{th}-order shear deformation theory with curvature effects”, *Steel Compos. Struct., Int. J.*, **21**(6), 1347-1368. https://doi.org/10.12989/scs.2016.21.6.1347

Brubak, L. and Hellesland, J. (2007a), “Approximate buckling strength analysis of arbitrarily stiffened, stepped plates”, *Eng. Struct.*, **29**(9), 2321-2333. https://doi.org/10.1016/j.engstruct.2006.12.002

Brubak, L. and Hellesland, J. (2007b), “Semi-analytical postbuckling and strength analysis of arbitrarily stiffened plates in local and global bending”, *Thin-Wall. Struct.*, **45**(6), 620-633. https://doi.org/10.1016/j.tws.2007.04.011

Brubak, L. and Hellesland, J. (2008), “Strength criteria in semi-analytical, large deflection analysis of stiffened plates in local and global bending”, *Thin-Wall. Struct.*, **46**(12), 1382-1390. https://doi.org/10.1016/j.tws.2008.03.013

Brubak, L., Hellesland, J. and Steen, E. (2007), “Semi-analytical buckling strength analysis of plates with arbitrary stiffener arrangements”, *J. Constr. Steel Res.*, **63**(4), 532-543. https://doi.org/10.1016/j.jcsr.2006.06.002

Ghaheri, A., Keshmiri, A. and Taheri-Behrooz, F. (2014), “Buckling and vibration of symmetrically laminated composite elliptical plates on an elastic foundation subjected to uniform in-plane force”, *J. Eng. Mech.*, **140**(7), 04014049. https://doi.org/10.1061/(ASCE)EM.1943-7889.0000760

Ghannadpour, S.A.M. and Ovesy, H.R. (2009a), “The application of an exact finite strip to the buckling of symmetrically laminated composite rectangular plates and prismatic plate structures”, *Compos. Struct.*, **89**(1), 151-158. https://doi.org/10.1016/j.compstruct.2008.07.014

Ghannadpour, S.A.M. and Ovesy, H.R. (2009b), “Exact post-buckling stiffness calculation of box section struts”, *Eng. Computat.*, **26**(7), 868-893. https://doi.org/10.1108/02644400910985224

Ghannadpour, S.A.M. and Barekati, M. (2016), “Initial imperfection effects on postbuckling response of laminated plates under end-shortening strain using Chebyshev techniques”, *Thin-Wall. Struct.*, **106**, 484-494. https://doi.org/10.1016/j.tws.2016.03.028

Ghannadpour, S.A.M. and Shakeri, M. (2018), “Energy based collocation method to predict progressive damage behavior of imperfect composite plates under compression”, *Latin Am. J. Solids Struct.*, **15**(4). https://doi.org/10.1016/j.compstruct.2018.04.011

Ghannadpour, S.A.M., Ovesy, H.R. and Zia-Dehkordi, E. (2014), “An exact finite strip for the calculation of initial post-buckling stiffness of shear-deformable composite laminated plates”, *Compos. Struct.*, **108**, 504-513. https://doi.org/10.1016/j.compstruct.2013.09.049

Ghannadpour, S.A.M., Kiani, P. and Reddy, J.N. (2017), “Pseudo spectral method in nonlinear analysis of relatively thick imperfect laminated plates under end-shortening strain”, *Compos. Struct.*, **182**, 694-710. https://doi.org/10.1016/j.compstruct.2017.08.076

Ghannadpour, S.A.M., Kurkaani Barvaj, A. and Tornabene, F. (2018a), “A semi-analytical investigation on geometric nonlinear and progressive damage behavior of relatively thick laminated plates under lateral pressure and end-shortening”, *Compos. Struct.*, **194**, 598-610. https://doi.org/10.1016/j.compstruct.2018.04.011

Ghannadpour, S.A.M., Shakeri, M. and Kurkaani Barvaj, A. (2018b), “Ultimate strength estimation of composite plates under combined in-plane and lateral pressure loads using two different numerical methods”, *Steel Compos. Struct., Int. J.*, **29**(6), 781-798. https://doi.org/10.12989/scs.2018.29.6.785

Hashin, Z. and Rotem, A. (1973), “A fatigue failure criterion for fiber reinforced materials”, *J. Compos. Mater.*, **7**, 448-464. https://doi.org/10.1177/002199837300700404

Hayman, B., Berggreen, C., Lundsgaard-Larsen, C., Delarche, A., Toftegaard, H., Dow, R.S., Downes, J., Misirlis, K., Tsouvalis, N. and Douka, C. (2011), “Studies of the buckling of composite plates in compression”, *Ships Offshore Struct.*, **6**(1-2), 81-92. https://doi.org/10.1080/17445302.2010.528283

Jiang, G., Li, F. and Li, X. (2016), “Nonlinear vibration analysis of composite laminated trapezoidal plates”, *Steel Compos. Struct., Int. J.*, **21**(2), 395-409. https://doi.org/10.12989/scs.2016.21.2.395

Jiang, H., Ren, Y., Liu, Z., Zhang, S. and Wang, X. (2018), “Evaluations of failure initiation criteria for predicting damages of composite structures under crushing loading”, *J. Reinf. Plastics Compos.*, **37**(21), 1279-1303. https://doi.org/10.1177/0731684418783847

Kar, V.R. and Panda, S.K. (2016), “Post-buckling behaviour of shear deformable functionally graded curved shell panel under edge compression”, *Int. J. Mech. Sci.*, **115**, 318-324. https://doi.org/10.1177/0731684418783847

Li, S.R., Batra, R.C. and Ma, L.S. (2007), “Vibration of thermally post-buckled orthotropic circular plates”, *J. Thermal Stresses*, **30**(1), 43-57. https://doi.org/10.1080/01495730600897161

Magnucki, K., Malinowski, M. and Kasprzak, J. (2006), “Bending and buckling of a rectangular porous plate”, *Steel Compos. Struct., Int. J.*, **6**(4), 319-333. https://doi.org/10.12989/scs.2006.6.4.319

Nejati, M., Dimitri, R., Tornabene, F. and Hossein Yas, M. (2017), "Thermal buckling of nanocomposite stiffened cylindrical shells reinforced by functionally Graded wavy Carbon NanoTubes with temperature-dependent properties", *Appl. Sci.*, **7**(12), 1223. https://doi.org/10.3390/app7121223

Ovesy, H.R. and Ghannadpour, S.A.M. (2011), "An exact finite strip for the initial postbuckling analysis of channel section struts", *Comput. Struct.*, **89**(19-20), 1785-1796. https://doi.org/10.1016/j.compstruc.2010.10.009

Ovesy, H.R., Ghannadpour, S.A.M. and Morada, G. (2005), "Geometric non-linear analysis of composite laminated plates with initial imperfection under end shortening, using two versions of finite strip method", *Compos. Struct.*, **71**(3-4), 307-314. https://doi.org/10.1016/j.compstruct.2005.09.030

Ovesy, H.R., Ghannadpour, S.A.M. and Nassirnia, M. (2015), "Post-buckling analysis of rectangular plates comprising Functionally Graded Strips in thermal environments", *Comput. Struct.*, **147**, 209-215. https://doi.org/10.1016/j.compstruc.2014.09.011

Panda, S.K. and Singh, B.N. (2013), "Nonlinear finite element analysis of thermal post-buckling vibration of laminated composite shell panel embedded with SMA fibre", *Aerosp. Sci. Technol.*, **29**(1), 47-57. https://doi.org/10.1016/j.compstruc.2014.09.011

Sun, Y., Li, S.R. and Batra, R.C. (2016), "Thermal buckling and post-buckling of FGM Timoshenko beams on nonlinear elastic foundation", *J. Thermal Stresses*, **39**(1), 11-26.

Taheri-Behrooz, F., Omidi, M. and Shokrieh, M.M. (2017), "Experimental and numerical investigation of buckling behavior of composite cylinders with cutout", *Thin-Wall. Struct.*, **116**, 136-144. https://doi.org/10.1016/j.tws.2017.03.009

Timoshenko, S.P. and Gere, J.M. (2009), *Theory of Elastic Stability*, Courier Corporation, New York, NY, USA.

Topal, U. (2013), "Application of a new extended layerwise approach to thermal buckling load optimization of laminated composite plates", *Steel Compos. Struct., Int. J.*, **14**(3), 283-293. https://doi.org/10.12989/scs.2013.14.3.283

Tornabene, F., Fantuzzi, N. and Bacciocchi, M. (2017), "Linear static behavior of damaged laminated composite plates and shells", *Materials*, **10**(7), 811. https://doi.org/10.3390/ma10070811

Yang, Q.J. and Hayman, B. (2015a), "Prediction of post-buckling and ultimate compressive strength of composite plates by semi-analytical methods", *Eng. Struct.*, **84**, 42-53. https://doi.org/10.1016/j.engstruct.2014.11.013

Yang, Q.J. and Hayman, B. (2015b), "Simplified ultimate strength analysis of compressed composite plates with linear material degradation", *Compos. Part B: Eng.*, **69**, 13-21. https://doi.org/10.1016/j.compositesb.2014.09.016

Yang, Q.J., Hayman, B. and Osnes, H. (2013), "Simplified buckling and ultimate strength analysis of composite plates in compression", *Compos. Part B: Eng.*, **54**, 343-352. https://doi.org/10.1016/j.compositesb.2013.05.017

CC